JOURNAL OF APPLIED ELECTROCHEMISTRY **27** (1997) 434–440

Visual observation of bubbles at horizontal electrodes and resistance measurements on vertical electrodes

K. QIAN, J. J. J. CHEN

Department of Chemical & Materials Engineering, The University of Auckland, New Zealand

N. MATHEOU

Comalco Research Centre, 15 Edgars Road, Thomstown, Melbourne, VIC 3074, Australia

Received 16 April 1996; revised 30 July 1996

A comparison was made of the bubbles formed on a horizontal bottom-facing electrode in a physical analogue model with those formed electrolytically. Bubbles formed in a physical analogue model by forcing air through a porous plate are larger, with wetted clear areas between bubbles. In contrast, electrolytically generated gas bubbles are smaller and the electrode surface is covered with a foamy layer of tiny bubbles. To measure the bubble resistance on horizontal electrodes, a method was developed for vertical electrodes so that the measurements may be validated by comparison with published data. Voltage fluctuations were measured and analysed using fast Fourier transform (FFT). The magnitude of the bubble impedance was obtained at a superimposed a.c. frequency f_0. The phase angle caused by the effects of the double layer capacitance and the faradaic impedance on bubble resistance were determined. The effects of the faradaic impedance and the double layer capacitance were shown to be negligibly small under experimental conditions.

List of symbols

A	cross-section area of electrode (m^2)
l_{AC}	anode–cathode distance (m)
f_0	frequency of imposed a.c. signal (Hz)
H	bath height (m)
l	path length between electrodes (m)
R	resistance (Ω)
T	period of the a.c. used (s)
V	voltage in the time domain (V)
V_{FFT}	peak voltages of impedance Z in the frequency domain (V)
X_C	capacitive reactance of double layer (Ω)
$x(t)$	function in the time domain
$y(t)$	function in the time domain
$z(t)$	resultant function of $x(t) + y(t)$
Z	impedance (Ω)

Greek letters

α	phase angle (deg.)
δ	bubble layer thickness (m)
ϵ	volume fraction of gas bubbles
ξ	phase shift (s)
ρ	bath resistivity (Ω m)

Subscripts

0	with no bubble present
1	reference resistance
2	resistance across electrodes
eff	effective, or, with bubbles present
f	faradaic

1. Introduction

In the Hall–Héroult process used in aluminium reduction cells, the electrodes are set in horizontal orientation and gas bubbles are generated on the underside of the anode which is immersed in the electrolyte. The presence of bubbles in the electrolyte directly in the path of current flow causes an increase in the electrolyte resistance and an effective increase in the true current density on the remaining wetted surface of the electrode, thus raising the overpotential. The term 'bubble resistance' generally refers to the increase in the electrolytic resistance in the interelectrode spacing due to the presence of gas bubbles [1, 2].

The observation of bubble behaviour and accurate measurements of bubble resistance in cells operating at elevated temperatures are difficult or near impossible, although some work on a reduction cell have been reported [3, 4]. Most measurements and analyses of bubble resistance refer to vertical electrodes [5, 6] and limited work was done for horizontal electrodes, such as those found in Hall–Héroult cells. Solheim and Thonstad [7] conducted an experiment on bubble resistance in a full scale physical analogue model of a Hall–Héroult cell and a correlation of bubble resistivity ratio was obtained as given in Equation 1. The most obvious difference in bubble behaviour between a physical analogue model and a reduction cell is the fact that gas bubbles in a physical

0021-891X © 1997 Chapman & Hall

analogue model are generated by forcing compressed air through a diffuser and the bubbles in a reduction cell are generated electrolytically. The effects due to the type of bubble generation needs to be investigated prior to the correlation, as given in Equation 1, being applied to a reduction cell:

$$\frac{\rho_{\text{eff}}}{\rho_0} = \left[1 + \frac{\delta}{l_{\text{AC}}}[(1-\epsilon)^{-1.5}] \times \frac{1}{\epsilon}\right] \qquad (1)$$

where the symbols are explained at the outset.

Dorin and Frazer [8] conducted experiments on bubble resistance in a laboratory-scale reduction cell with a 24 mm diameter anode. The effect of the bubble layer on bubble resistance was investigated over a range of l_{AC}. The effect of scale on bubble resistance needs to be known before the results obtained in such a scaled reduction cell may be applicable to an operating reduction cell.

Hine and Murakami [6] conducted experiments using vertical electrodes made of stainless steel 89 cm long and 3 cm wide. A 2M NaOH solution was the electrolyte. The anode–to–cathode gap was varied in the range 0.5–3 cm and the current density 0.1–2 A cm^{-2}. Hine and Murakami concluded from their data that Bruggeman equation [9], as given in Equation 2, is valid:

$$\frac{\rho_{\text{eff}}}{\rho_0} = (1-\epsilon)^{-1.5} \qquad (2)$$

In this paper we present observations on the difference between simulated and electrolytically generated gas bubbles on horizontal electrodes. We also develop a method of bubble resistance measurement which is based on the use of FFT to analyse fluctuating voltage signals arising from an imposed a.c. signal of known frequency. As there are no data for horizontal electrodes for comparison with our method of measurement, our data on vertical electrodes are compared with a published correlation. In future publications, studies on horizontal, or near-horizontal, electrodes will be reported, with applications to Hall–Héroult cells.

2. Bubble behaviour

In an attempt to gain a better understanding of the bubble behaviour in an electrolytic cell, and particularly in a Hall–Héroult cell with horizontal electrodes, a physical analogue model and a low temperature electrolytic cell of the same scale were used for bubble behaviour observations.

A schematic diagram of the physical analogue model used in this work is shown in Fig. 1. The simulated anode with the bottom surface made of porous bronze plate had a working area of 100 mm × 40 mm. The bubbles under the simulated anode were generated by forcing compressed air through the porous bronze plate.

A schematic diagram of the low temperature electrolytic cell is shown in Fig. 2. The carbon anode is made out of a graphite block with working dimensions of 100 mm × 40 mm. A split carbon cathode, consisting of two blocks of graphite placed on either side of the anode, was used to allow observations of the bubble behaviour from a position directly below the anode. A 2M NaOH aqueous solution was used as the electrolyte.

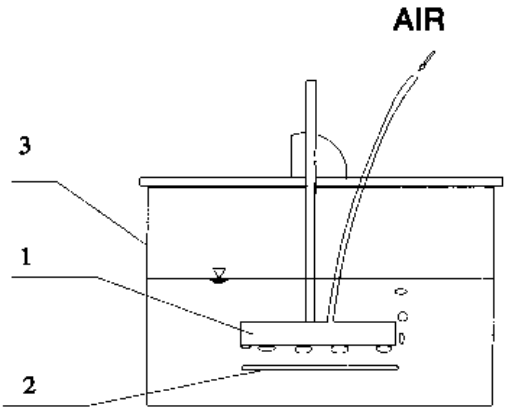

Fig. 1. Schematic diagram of the physical analogue model. Key: (1) simulated anode; (2) simulated cathode; (3) tank.

The bubble behaviour is affected by the properties of the solution and the mechanism of bubble generation. As we are interested in bubble generation in the same solution, a 2M NaOH solution was also used in the physical analogue model shown in Fig. 1.

Typical bubbles observed in the physical analogue model of Fig. 1 are shown in Fig. 3. It is observed that a few large bubbles are dispersed under the anode, and there are clear areas between bubbles that are totally wetted by the electrolyte.

Typical bubbles observed in the low temperature electrolytic cell of Fig. 2 are shown in Fig. 4. It may be seen that the entire underside of the anode is covered by a foamy layer of tiny bubbles as compared to the clear areas between larger bubbles observed in the physical analogue model. The average diameter of these fine bubbles is less than 0.5 mm. In addition, a few large bubbles are dispersed in this foamy layer of fine bubbles. The bubble size in the low temperature electrolytic cell is smaller than the bubble size in the

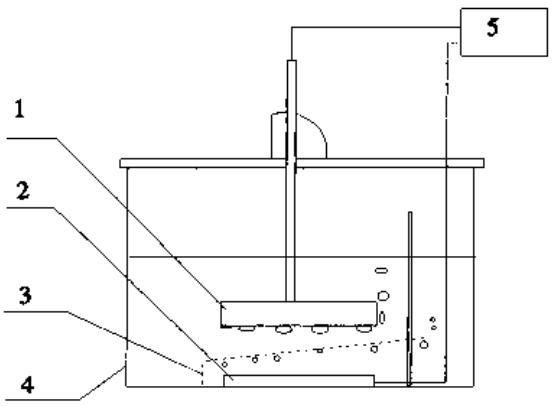

Fig. 2. Schematic diagram of the low temperature electrolytic cell. Key: (1) carbon anode; (2) split carbon cathode; (3) screen; (4) tank; (5) d.c. power supply.

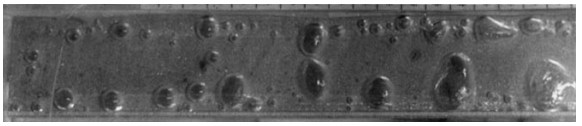

Fig. 3. Bubble pattern in the physical analogue model. Full scale (as shown in plate) is 40 mm × 200 mm.

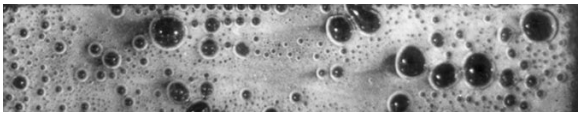

Fig. 4. Bubble pattern in low temperature electrolytic cell. Full scale (as shown in plate) is 40 mm × 200 mm.

physical analogue model. The volumes of these large bubbles increase as the bubbles travel and coalescence occurs.

In Figs 3 and 4, the gas evolution rate correspond to a current density of 0.45 A cm^{-2} and the anodes are inclined at about 2° to the horizontal to facilitate movement of the gas bubbles and to more closely simulate actual operating situations where the anode bottom surface is slightly inclined due to the slightly heaved metal surface.

There is a distinct difference between the bubble pattern formed under the simulated anode as shown in Fig. 3 and the bubble pattern under the carbon anode as shown in Fig. 4. Thus, even though the same solution was used (i.e., with identical surface tension and viscosity) the bubbles formed were different depending on whether the bubbles were generated electrolytically, and thereby impact charges to the gas bubbles, or by a simulated anode through which an inert gas was passed.

It is expected that the bubble resistance is strongly influenced by the bubble shape and size, as well as size distribution. Thus, it is argued that correlations such as that shown in Equation 1 cannot be reliably applied to a reduction cell unless the bubble behaviour is known for a real reduction cell and is adequately considered in the derivation of the correlation.

3. Measurement method

Ideally, to allow comparison of the resistance data obtained in the physical analogue model and the low temperature electrolytic cell, the same measurement method should be used in both cases. Currently, there are two established methods of bubble measurement, one uses d.c. and the other uses a.c.

Using d.c. the current interrupter technique was used by Newman [10] and Hyde and Welch [11]. The Luggin probe method was used by Hine and Murakami [6]. In our experiments, particularly for the physical analogue model, the d.c. method was not suitable because of electrolytic bubble formation.

When an a.c is used, it is superimposed on the d.c. at various a.c. frequencies. The resistances obtained at the various imposed a.c. frequencies are plotted and the resistance at infinite a.c. frequency determined. This method, often referred to as the a.c. impedance method, is difficult to apply in our experiments for the following reasons:

(i) Haupin and Frank [12] suggested that the a.c. frequency effect is complex and, at high frequencies, the bubbles are bypassed, hence behaving like small capacitors. At low frequencies polarization resistance predominates.
(ii) Thonstad [13] stated that the ohmic voltage drop between the anode and the reference electrode could not be accurately determined by the a.c. impedance method at current densities above 0.15 A cm^{-2} because gas bubbles caused potential oscillations.
(iii) Dewing and van der Kouwe [14] pointed out that previous workers appear to have ignored the fact that the faradaic resistance is also included when the a.c. impedance method was used.
(iv) Dorin and Frazer [8] conducted experiments on bubble resistance measurement using the a.c. impedance method. The phase difference was measured so as to isolate the effect of the double layer capacitance.

Thus, it appears, particularly with regards to Haupin and Frank [12] and Thonstad [13] that the existing methods of resistance measurement are not suitable for bubble resistance measurement. A new method is therefore developed which can be used to accurately measure the bubble resistance at high current density, and is able to isolate the effects of the faradaic impedance and the double layer capacitance.

3.1. *Bubble impedance ratio measured using FFT*

FFT theory [15] shows that if $x(t)$ and $y(t)$ have different frequencies, the magnitudes of these functions may be determined at their respective frequencies in the frequency domain. In our work, if $x(t)$ is an imposed a.c. of 50 Hz and $y(t)$ is the d.c. signal, the resultant signal $z(t) = x(t) + y(t)$ in the time domain will not allow accurate measurements of the magnitude of $x(t)$. However, with the application of FFT, the magnitudes of $x(t)$ and $y(t)$ may be determined at their respective frequencies in the frequency domain. The magnitude of the peak voltage V_{FFT} at 50 Hz in the frequency domain is a measure of the magnitude of the a.c. signal of 50 Hz in the time domain.

Given two series impedances Z_1 and Z_2, application of FFT gives

$$\frac{Z_2}{Z_1} = \frac{V_{\mathrm{FFT2}}}{V_{\mathrm{FFT1}}} \tag{3}$$

This shows that the ratio of Z_1 and Z_2 may be calculated by the values of V_{FFT1} and V_{FFT2} in the frequency domain. If Z_2 represents the impedance of electrolyte with bubbles present, and Z_1 represents the impedance of electrolyte with no bubble present, then the bubble impedance ratio is given by the ratio

of Z_2 to Z_1. It is, however, necessary to isolate the bubble resistivity ratio from the bubble impedance ratio measured by the above procedure.

To compare the effects of bubble resistance, the bubble resistivity ratio, which is the ratio of the resistivity of electrolyte with bubbles present to the resistivity of electrolyte with no bubble present, is widely used in the literature.

3.2. *Effect of double layer capacitance*

In the measurement of the bubble resistance in a physical analogue model and in a low temperature electrolytic cell, a double layer exists at the interface between the electrode and the solution and it behaves as a capacitor. The voltage component due to the capacitive reactance of double layer influences the total voltage measured. The resistance, R, is related to the impedance, Z, by

$$R = Z \cos \alpha \tag{4}$$

Thus, if the phase angle α and the impedance Z are known, the resistance R can be calculated using Equation 4.

3.3. *Conversion of resistivity ratio from impedance ratio*

If Z_1 is a resistance with no capacitance or inductance, and Z_2 is an impedance which includes a capacitance, the corresponding voltages V_1 and V_2 measured in the time domain are shown in Fig. 5. The phase angle is given by Equation 5 [16].

There is a phase shift ξ between the two curves Z_1 and Z_2 as shown in Fig. 5, and the phase angle α (in degrees) between Z_1 and Z_2 is given by

$$\alpha = \frac{\xi}{T} \times 360^\circ \tag{5}$$

As $R_1 = Z_1$ when the impedance consists solely of a resistance, and $R_2 = Z_2 \cos \alpha$,

$$\frac{R_2}{R_1} = \frac{Z_2 \cos \alpha}{Z_1} \tag{6}$$

The resistance R is related to the specific resistance ρ by

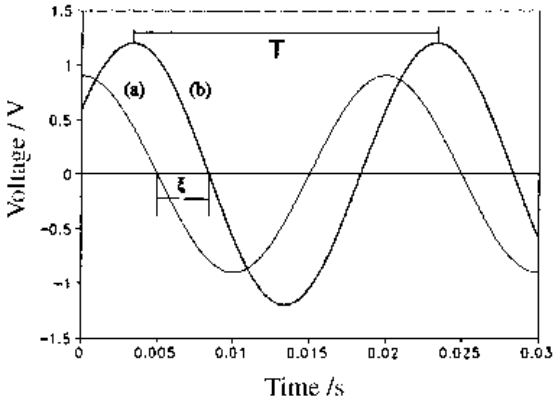

Fig. 5. A phase shift ξ between two curves Z_1 (a) and Z_2 (b). T is the period.

$$R = \rho \frac{l}{A} \tag{7}$$

where l and A are, respectively, the distance between the electrodes and the cross-sectional area of the working surface of the electrodes.
When $l_1 = l_2$ and $A_1 = A_2$,

$$\frac{\rho_2}{\rho_1} = \frac{R_2}{R_1} \tag{8}$$

Hence, for an electrolytic cell, if ρ_{eff} and ρ_0 are, respectively, the resistivity when bubbles are present and absent, then

$$\frac{\rho_{\text{eff}}}{\rho_0} = \frac{R_{\text{eff}}}{R_0} = \frac{Z_{\text{eff}} \cos \alpha}{Z_0} \tag{9}$$

The bubble resistivity ratio can therefore be calculated using Equation 9.

3.4. *Effect of faradaic impedance*

When an a.c. signal is superimposed on a d.c. in an electrolytic cell, a faradaic impedance will be generated due to concentration polarization and activation polarization which are explained in detail by Koryta *et al.* [17] and Oldham and Myland [18]. Delahay [19] presented an analysis showing that the double layer capacitance is in parallel with the faradaic impedance and these two components are in series with the solution resistance R of the cell as depicted in Fig. 6.

Z_{total}, total impedance of the double layer capacitance, X_C, and the faradaic impedance, Z_f, is given by

$$Z_{\text{total}} = \frac{Z_f X_C}{Z_f + X_C} \tag{10}$$

Because the faradaic impedance and the double layer capacitance are in parallel, the total impedance Z_{total} is always less than either of these two components.

The bubble resistance may be affected by the faradaic impedance, Z_f, under the following conditions:

(i) If the double layer capacitance, X_C, is very small, no matter how large the faradaic impedance Z_f, the total impedance Z_{total} is small. Hence, the effect due to the faradaic impedance on the bubble resistance is limited.

(ii) If the faradaic impedance, Z_f, is large and the double layer capacitance, X_C, is larger than the faradaic impedance, a large part of the a.c. passes through the faradaic impedance. The phase shift measured will be caused mainly by

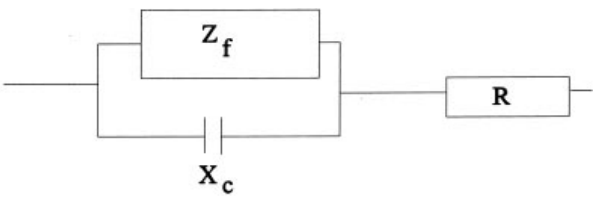

Fig. 6. Equivalent circuit of electrolytic cell with double layer capacitance (X_C), faradaic impedance (Z_f) and solution resistance (R).

the faradaic impedance. In this case, the phase shift may be small, but the resistances measured include not only the resistance of the solution used but also the resistance due to the faradaic impedance. Dewing and van der Kouwe [14] conducted an experiment and the effect of the faradaic impedance on overpotential was calculated using the Taylor's series. As the purpose of our work is to study the bubble resistance, the effect of the faradaic impedance on the resistance needs to be isolated.

When an a.c. signal whose voltage is much less than the Nernst potential of the solution is passed through a low temperature electrolytic cell in the absence of a d.c., there is no electrochemical reaction and therefore no polarization. Hence, the faradaic impedance does not occur. The phase shift measured is due entirely to the double layer capacitance X_C. When an a.c. signal and a d.c. pass through the low temperature electrolytic cell simultaneously, and if the d.c. voltage is higher than the Nernst potential of the solution used, there will be an electrochemical reaction and a faradaic impedance will be present. The phase shift results from the total impedance Z_{total} of the faradaic impedance Z_f and the double layer X_C. Comparing the phase shifts measured with and without a d.c., the faradaic impedance can be isolated.

4. Tests in a low temperature electrolytic cell

To examine the accuracy of the FFT method of measurement, outlined in previous Section, published results must be used. However, the only available data are for electrodes placed in the vertical position. Consequently, instead of using the equipment shown in Fig. 2, the arrangement was redesigned for use with vertical electrodes. A schematic diagram of the low temperature electrolytic cell with vertical electrodes is shown in Fig. 7. The design of this test equipment closely follows that of Hine and Murakami [6].

For the analysis of the results obtained, the Bruggeman equation will be used as Tobias [20] proposed its use for correlating the resistivity against gas void fraction in electrolytic cells. Hine and Murakami [6] also concluded that the Bruggeman equation, as given in Equation 2, is valid.

Both the anode (1) and the cathode (2) were stainless steel 20 cm long × 1.3 cm wide × 0.1 cm thick. Two plastic spacers (3) with dimensions 1.3 cm × 2 cm × 1.5 cm were fixed at the top and bottom ends of the electrodes to ensure a fixed anode-to-cathode gap. A reference resistance (5), consisting of a 0.8 cm diameter graphite roll with a resistance of 0.291 Ω, as measured by a PM 6303 PCL Philips meter, was used. Two polystyrene backing blocks (7) were used to reduce the working section so as to allow more electrolyte to be displaced by gas bubbles during electrolysis, increasing the accuracy of the void fraction measurement. A 2 M NaOH solution (10) was used as the electrolyte. The anode-to-cathode gap was 2 cm, and the current density was varied from 0.2–1.5 A cm^{-2}.

The cell was designed such that excess liquid overflowed when a height H_{eff} was reached. When the current was switched on, bubbles were generated and the electrolyte overflowed until the electrolyte–gas mixture reached a height of H_{eff}. When the current was switched off, bubbles disengaged and the liquid electrolyte reached a new height, H_0. Thus, the void fraction ϵ during electrolysis can be calculated by Equation 11:

$$\epsilon = \frac{H_{eff} - H_0}{H_0} \tag{11}$$

Typical voltages measured in the time domain across the reference resistance V_1 and the cell V_2 are shown in Fig. 8. The peak voltages V_{FFT1} and V_{FFT2} in the frequency domain after the application of FFT are shown in Fig. 9. Values for V_{FFT1} and V_{FFT2} such as given in Fig. 9 were used to calculate the ratio Z_2/Z_1 using Equation 3.

The procedure was applied using the equipment shown in Fig. 7 for a range of d.c. values, including zero d.c. for no bubble generation.

The phase angle caused by the double layer capacitance in the low temperature electrolytic cell was

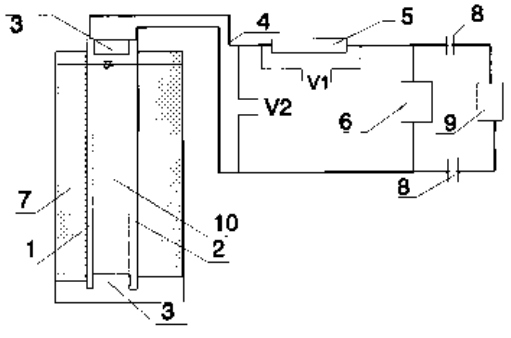

Fig. 7. Schematic diagram of the low temperature electrolytic cell with vertical electrodes. Key: (1) anode; (2) cathode; (3) plastic spacer; (4) copper conductor; (5) reference resistance (0.291 Ω); (6) d.c. power supply; (7) polystyrene backing block; (8) capacitor; (9) a.c. signal source; (10) electrolyte.

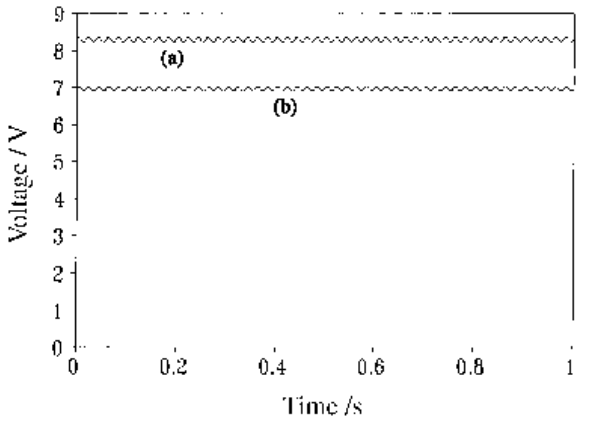

Fig. 8. Voltages V_1 (a) and V_2 (b) measured in the low temperature electrolytic cell in the time domain.

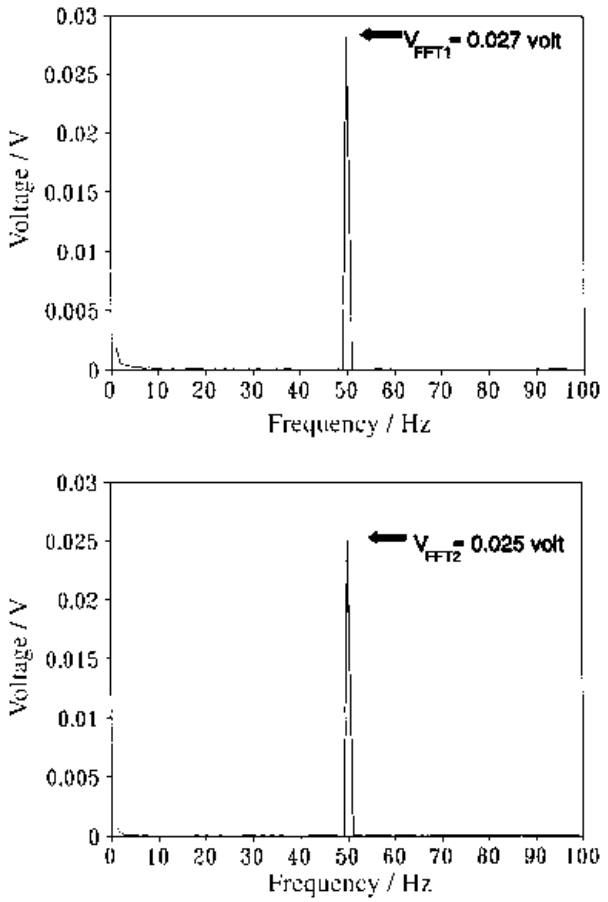

Fig. 9. Peak voltages V_{FFT1} and V_{FFT2} obtained by transforming V_1 and V_2 in Fig. 8 into the frequency domain.

calculated using Equation 5 to be 4.4° ($\cos 4.4° = 0.997$); similarly, the phase angle caused by the total impedance Z_{total} in the low temperature electrolytic cell was calculated to be about 4°. This shows that the effect of the faradaic impedance on the bubble resistance in our experiment is negligibly small. The resistance ratio was calculated using the Equation 6, and in our work, the resistivity ratio R_{eff}/R_0 was equal to the resistance ratio ρ_{eff}/ρ_0 as given in Equation 9. The void fraction ϵ was calculated using Equation 11.

Bruggeman equation was used to verify the application of the FFT technique. The ratio ρ_{eff}/ρ_0 obtained by actual experimental measurements and the ratio ρ_{eff}/ρ_0 calculated using Bruggeman equation are compared in Table 1 and plotted in Fig. 10.

Table 1. Void fraction against resistivity ratio ρ_{eff}/ρ_0

Void fraction, ε	*Our work ρ_{eff}/ρ_0*	*Bruggeman ρ_{eff}/ρ_0*	*Error /%*
0.11	1.21	1.18	+ 2.7
0.12	1.23	1.20	+ 2.3
0.22	1.49	1.45	+ 2.7
0.27	1.56	1.62	– 3.6
0.32	1.70	1.77	– 4.0
		average error = 3.1%	

It is clear from Fig. 10 that the resistivity ratios obtained from an electrolytic cell with vertical electrodes using the FFT method of measurement is in agreement with Bruggeman equation (average error 3.1% and maximum error 4.0%). This substantiates the findings of Tobias [21] and Hine and Murakami [6]. It should be noted that the data obtained by Hine and Murakami for correlating the Bruggeman equation were obtained using a d.c. measurement method.

5. Conclusion

It has been shown that bubbles generated electrolytically on horizontal anodes are clearly different from bubbles generated by forcing air through a simulated anode. This difference in bubble formation and flow pattern is expected to result in different resistivity ratios, even under conditions of equal gas evolution rate and similar solution properties.

A method of bubble resistance measurement was developed by using FFT to analyse the fluctuating voltage signals due to an imposed a.c. signal. The components of impedance due to the effects of the faradaic impedance and the double layer capacitance were also isolated. For the conditions of our experiments, the effect of double layer capacitance on bubble resistance was shown to be negligibly small, although the phase angles obtained in this work were slightly larger than those obtained by Dorin and Frazer in their laboratory-scale cell [8]. The effect of the faradaic impedance on the bubble resistance was

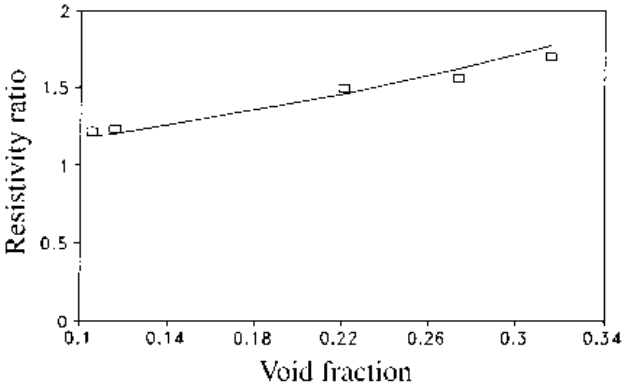

Fig. 10. Resistivity ratio ρ_{eff}/ρ_0 against void fraction. Key: (——) Bruggeman equation; (□) this work.

also shown to be negligibly small under the conditions described.

Acknowledgements

The authors are grateful to Dr E. Frazer of CSIRO, Institute of Minerals, Energy and Construction, Australia, for valuable discussions and suggestions. Discussions with Professor B. J. Welch and Dr M. P. Taylor have been most appreciated. Comalco Research Centre and The University of Auckland Research Committee provided support for this work.

References

[1] K. Grjotheim and B. J. Welch, 'Aluminium Smelting Technology', 2nd edn, Aluminium Verlag (1988), pp. 175–182.
[2] W. H. Haupin, *in* 'Production of Aluminium and Alumina', 2nd edn (edited by A. R. Burkin), John Wiley & Sons, Chichester (1987) pp. 150–58.
[3] W. E. Haupin, *J. Metals* Oct. (1971) 46–9.
[4] G. J. Houston, M. P. Taylor, D. J. Williams and K. Grjotheim, *Light Metals 1988* 117th Annual Meeting of AIME (1988) 641–5.
[5] B. E. Bongenaar-Schlenter, L. J. J. Janssen, S. J. D. van Stralen and E. Barendrecht, *J. Appl. Electrochem.* **15** (1985) 537–48.
[6] F. Hine and K. Murakami, *J. Electrochem. Soc.* **127** (1980) 292–7.
[7] A. Solheim and J. Thonstad, *Light Metals 1986*, 115th Annual Meeting of AIME (1986) 379–403.
[8] R. Dorin and E. J. Frazer, *J. Appl. Electrochem.* **23** (1993) 933–42.
[9] D. A. G. Bruggeman, *Ann. Phys.* **24** (1935) 636–64.
[10] J. Newman, *J. Electrochem. Soc.* **117** (1970) 507–8.
[11] T. M. Hyde and B. J. Welch, CHEMECA 92, Canberra, Australia, 27–30 Sept. (1992), **2**, pp. 161–8.
[12] W. E. Haupin and W. B. Frank, *in* 'Comprehensive Treatise of Electrochemistry', **2**, (edited by O'M. Bockris, *et al.*, Plenum Press, London (1981) pp. 301–25.
[13] J. Thonstad, *Electrochim. Acta* No. **15** (1970) 1569–80.
[14] E. W. Dewing and E. Th. van der Kouwe, *J. Electrochem. Soc.* **122** (1975) 358–63.
[15] R. W. Ramire, 'The FFT, Fundamentals and Concepts', Prentice-Hall, Englewood Cliffs, NJ (1985), pp. 17–59.
[16] G. E. Williams and B. J. Prinmore, 'Electrical Engineering', Heinemann, London (1963), pp. 182–3.
[17] J. Koryta, J. Dvorak and L. Kavan, 'Principles of Electrochemistry', J. Wiley & Sons, New York 2nd edn (1993) pp. 301–2.
[18] K. B. Oldham and J. C. Myland, 'Fundamentals of Electrochemical Science', Academic Press, San Diego (1994) pp. 367–73.
[19] P. Delahay, 'New Instrumental Methods in Electrochemistry', Interscience Publication, New York (1954) pp. 146–8.
[20] C. W. Tobias, *J. Electrochem. Soc.* **106** (1959) 833–8.